Spin-Orbital Correlated Dynamics in the Spinel-Type Vanadium Oxide MnV_2O_4

Keisuke Matsuura,[1,*] Hajime Sagayama,[2] Amane Uehara,[3] Yoichi Nii,[4] Ryoichi Kajimoto,[5] Kazuya Kamazawa,[6] Kazuhiko Ikeuchi,[6] Sungdae Ji,[6,†] Nobuyuki Abe,[1] and Taka-hisa Arima[1]

[1]*Department of Advanced Materials Science, the University of Tokyo, Kashiwa 277-8561, Japan*
[2]*Institute of Materials Structure Science, High Energy Accelerator Research Organization, Tsukuba, Ibaraki 305-0801, Japan*
[3]*Department of Applied Physics, the University of Tokyo, Tokyo 113-8656, Japan*
[4]*Department of Basic Science, the University of Tokyo, Komaba 153-8902, Japan*
[5]*J-PARC Center, Japan Atomic Energy Agency, Tokai, Ibaraki 319-1195, Japan*
[6]*Neutron Science and Technology Center, Comprehensive Research Organization for Science and Society (CROSS), Tokai, Ibaraki 319-1106, Japan*

(Received 2 September 2016; published 5 July 2017)

We investigate the magnetic dynamics in the spinel-type vanadium oxide MnV_2O_4. Inelastic neutron scattering around 10 meV and a Heisenberg model analysis have revealed that V^{3+} spin-wave modes exist at a lower-energy region than previously reported. The scattering around 20 meV cannot be reproduced with the spin-wave analysis. We propose that this scattering could originate from the spin-orbital coupled excitation. This scattering is most likely attributable to V^{3+} spin-wave modes, entangled with the orbital hybridization between t_{2g} orbitals.

DOI: 10.1103/PhysRevLett.119.017201

A macroscopic ordered state, accompanied by symmetry breaking, is characterized by its order parameters [1]. The low-energy dynamics from the ordered state corresponding to the modulation of the order parameters is represented by a quantized boson known as a quasiparticle. In general, physical phenomena can be described by the creation, annihilation, and motion of quasiparticles. A phonon is a particle that quantizes the deviation from the equilibrium position of an atom. A magnon is a particle that quantizes the fluctuation from the magnetic ordered state, and transports the change in spin angular momentum ΔS via a magnetic exchange interaction. A basic quasiparticle, such as a phonon and magnon, is composed of a single degree of freedom. However, in the field of condensed matter physics, quasiparticles related to two or more degrees of freedom have drawn considerable attention [2,3]. Here, we focus on the dynamical coupling between orbital and spin degrees of freedom in strongly correlated electron systems, which is an example for such a coupled quasiparticle. The orbital degree of freedom plays an important role in novel physical phenomena such as high-T_c superconductivity [4], the colossal magnetoresistance effect [5], the giant magnetoelectric effect [6,7], etc., via the coupling with charge, spin, and lattice degrees of freedom. A nonlocal quasiparticle in the orbital sector is termed an orbiton. The orbiton is a dynamic modulation of the shape of electronic clouds. The change in orbital angular momentum ΔL propagates via the transfer integral term between neighboring transition metal ions [8]. The first experimental observation of an orbiton was reported in $LaMnO_3$ [9,10], followed by several reports on perovskite-structure materials such as $KCuF_3$ [11], $R TiO_3$ (R = La, Y) [12,13], and $NdVO_3$ [14,15], and a one-dimensional system, Sr_2CuO_3 [16]. In these compounds, the orbital and magnetic transition temperatures are well separated, and most of the orbital ordered phases are antiferromagnetic. The strong coupling between the orbital and lattice degrees of freedom hinders the observation of spin-orbital coupled waves. Recently, the spin-orbital entangled excited state was suggested using far infrared and terahertz absorption measurements of $FeSc_2S_4$, in which the ground state is proposed to be a spin-orbital liquid [17].

Therefore, we chose the spinel-type vanadium oxides AV_2O_4 (A = Al [18], Zn [19], Mg [20,21], Cd [22], Mn [23–31], Fe [28,32–35], Co [36–38]) [Fig. 1(a)] for observing such spin-orbital coupled waves. The d orbitals of the V-site ion, coordinated by an oxygen octahedron, are split into lower-lying t_{2g} orbitals and higher-lying e_g orbitals. Owing to the edge-sharing structure between the oxygen octahedra, the orbitals at neighboring V^{3+} ions directly overlap each other, thus enhancing the Kugel-Khomskii type spin-orbital interactions [39] between V^{3+} ions. Furthermore, in the t_{2g} orbital degenerate system in the O_h symmetry ligand field, the relativistic spin-orbit interaction (SOI) can compete with the relatively weak Jahn-Teller interaction [40,41]. In MnV_2O_4, Mn^{2+} with a high-spin configuration ($S = \frac{5}{2}$) on a tetrahedral site has no orbital degeneracy. During cooling, a phase transition takes place into a collinear ferrimagnetic order at $T_C = 58$ K. At a lower temperature, $T_{OO} = 53$ K, a structural phase transition takes place from the cubic to the tetragonal structure, accompanied by the V^{3+}-site orbital order [23,24,42], in which the $|yz\rangle$ and $|zx\rangle$ orbitals are alternately arranged along the c axis, as shown in Fig. 1(c)

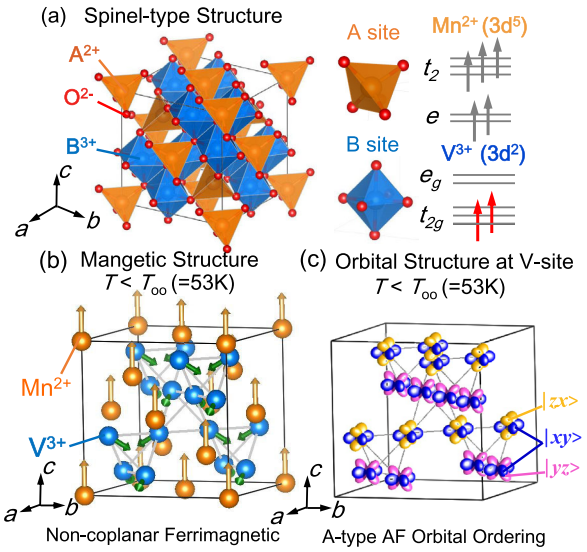

FIG. 1. (a) Crystal structure of the spinel-type oxide MnV_2O_4. Each A-site ion is surrounded by an oxygen tetrahedron. Each B site is coordinated by an oxygen octahedron. The V^{3+} ion has orbital degeneracy in the t_{2g} orbital. (b) Magnetic structure in the tetragonal phase ($c < a$) below $T_{OO} = 53$ K. The spin moment of the Mn^{2+} ion is parallel to the c axis and that of the V^{3+} ion is in the opposite direction with a canted angle of 60° from the $-c$ axis [25]. (c) Proposed A-type antiferroic (AF) orbital structure at V sites below $T_{OO} = 53$ K [24,28,40,43].

[24,28,31,40,43]. Simultaneously, the magnetic structure changes into a noncoplanar ferrimagnetic order [25] [Fig. 1(b)]. The characteristics of this orbital structure lie in the ferroic and antiferroic arrangements of the orbitals along the $[110]_c$ and $[101]_c$ directions, respectively. Here, the subscript c indicates the unconventional face-centered tetragonal unit cell to avoid the 45° rotation of the $\vec{a}$ and $\vec{b}$ vectors. The orbital and ferrimagnetic order coexists in MnV_2O_4, which may provide a stage for controlling the orbital degree of freedom through the spin sector. Chung *et al.* assigned the magnetic excitations in MnV_2O_4 below 10 meV to Mn^{2+} modes and those above 17 meV to V^{3+} modes by inelastic neutron scattering (INS) [26,27]. A recent Raman scattering measurement ($\mathbf{Q} = 0$) by Gleason *et al.* [30], however, found another excitation around 9–10 meV, which was not clearly observed by Chung *et al.* They also observed the anomalous two-magnon scattering around 20 meV, the energy shift of which increased towards T_{OO}. The ultrasound measurement of MnV_2O_4 in a magnetic field revealed elastic softening above T_{OO}. This softening is correlated with the magnetic phase transition, indicating a spin-orbital coupled fluctuation above T_{OO} [29].

In the present study, we investigated the magnetic dynamics of MnV_2O_4 by INS in the larger reciprocal lattice space. Using a Heisenberg model analysis, we found that the magnetic scattering assigned to V^{3+} modes exists around ~10 meV. Finally, a possible origin of the magnetic scattering around 20 meV, which cannot be reproduced with the Heisenberg model, is discussed.

Single crystals were grown using the floating-zone method [31]. They were characterized by powder x-ray diffraction and magnetization measurements. Four crystal bars, having a total mass of 10 g, were coaligned using backscattering Laue photographs. The INS was carried out using the 4SEASONS spectrometer at MLF, J-PARC [44]. Two-dimensional detectors and multiple E_i's enable the efficient measurement of large volumes of reciprocal space [45,46]. The incident energies of the neutrons were selected as 73, 34, 19, and 12 meV by a Fermi chopper. The sample was rotated around $[001]_c$ by a 0.5-deg step per 15 min. The temperature was maintained at 5.6 K. Using the software UTSUSEMI [47], we extracted the value proportional to the dynamical structure factor. In addition, the intensity was divided by the Bose factor. The binning parameters were 0.1 (r.l.u.) for H, K, and L and 0.4 meV for the energy.

In order to identify the spin-wave modes from the experimentally obtained intensity data, we performed a semiclassical spin-wave analysis in MnV_2O_4 [48]. A unit cell consists of six magnetic ions, Mn_1, Mn_2, V_1, V_2, V_3, and V_4. In the ground state, the canted angle between the Mn^{2+} and V^{3+} moments was assumed to be 120° [25,48]. Since the XMCD measurement of MnV_2O_4 suggests that $\langle L_z \rangle$ is negligibly small (< 0.15), the orbital angular momentum would be almost quenched in the ground state [31,49] (see also the Supplemental Material [48]). Therefore, the Hamiltonian $\hat{\mathcal{H}}$ is given by

$$\hat{\mathcal{H}} = \sum_{i,j} J_{i,j} \vec{\mathbf{S}}_i \cdot \vec{\mathbf{S}}_j + D \sum_{i \in V} (S_i^d)^2. \quad (1)$$

Here, $J_{i,j}$ is the isotropic exchange interaction between the sites i and j, i.e., J_1 between neighboring Mn^{2+}-V^{3+}, J_2 between the pair V^{3+}-V^{3+} along $[110]_c$, and J_3 between V^{3+}-V^{3+} along $[101]_c$. D is the single ion anisotropy of the V^{3+} ions. d is either x or y, depending on the alternative orbital order. The schematic representations of all six spin-wave modes at the Γ point, in the ascending order of energy, are represented in Fig. 2. The lowest energy mode is the Mn^{2+} acoustic mode, depicted in Fig. 2(a). The time evolutions of the two Mn^{2+} spin moments are in phase with each other. In the Mn^{2+} optical mode [Fig. 2(b)], the time evolutions of the Mn_1 and Mn_2 spin moments are out of phase. In V^{3+} modes 3 and 4, the major axes of the ellipsoid in spin precession are parallel to the $\vec{a}$ or $\vec{b}$ directions [Figs. 2(c) and 2(d)]. In contrast, those in V^{3+} modes 5 and 6 are mainly along the c axis. In other words, V^{3+} modes 5 and 6 are dominated by the spin oscillation ΔS_z along the z axis [Figs. 2(e) and 2(f)]. V^{3+} mode 5, which has a lower energy (~14 meV) is a coupled mode of the V^{3+} and Mn^{2+} modes.

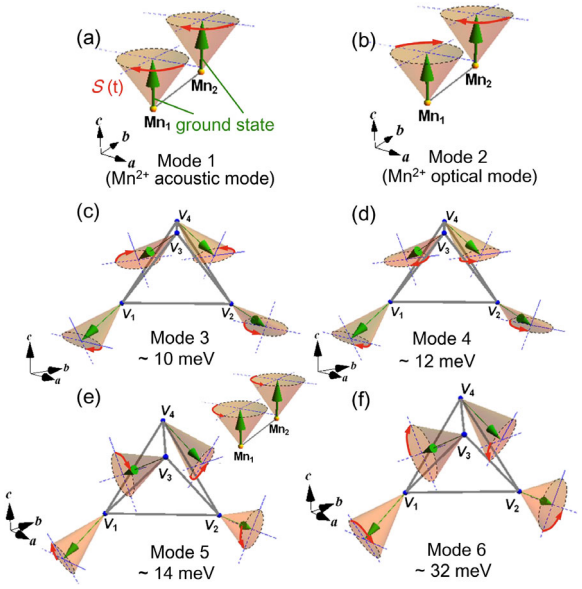

FIG. 2. Six spin-wave modes in MnV_2O_4 at the Γ point. Two of them are Mn^{2+} spin precession modes (mode 1 and mode 2) and the others are V^{3+} modes (modes 3–6).

Figures 3(a)–3(c) show the experimental results of the INS at $E_i = 34$ meV and $T = 5.6$ K along three high symmetry axes: (a) $[hhh]_c$, (b) $[hh0]_c$, and (c) $[h00]_c$. The corresponding calculations are shown in Figs. 3(d)–3(f). We averaged the calculated intensity from a multiple-domain sample for comparison with the experimental results. The energy region below 17 meV was reproduced well by our intensity calculation. In Fig. 3(a), we can observe not only an acoustic branch from the Γ point (111) but also a clear optical branch with an 8–9 meV energy gap. In our calculation, the former and the latter branches correspond to the Mn^{2+} acoustic and optical modes, respectively. In addition, the dispersive inelastic scattering intensity around 10 meV is newly observed along $[hh0]$ in the present study [Fig. 3(b)]. Figure 3(g) shows the energy-intensity plot at $[hh0]$ ($h = 1.8$–2.2), at $E_i = 19$ meV. An inelastic scattering peak with a width of ~3 meV is observed around 10 meV. Considering the energy resolution to be less than 1 meV [48], this broad peak may be ascribed to at least two branches. Our calculation suggests that the lower- and higher-energy branches should be assigned to the Mn^{2+} optical mode [Fig. 2(b)] and V^{3+} mode 3 [Fig. 2(c)], respectively. The lowest energy of the V^{3+} spin waves would extend to 10 meV rather than to 17 meV reported by Chung *et al.* [26]. In Figs. 3(b) and 3(c), we can see a dispersive mode with a large scattering intensity around 20 meV at both (2,2,0) and (4,0,0). This scattering was also observed at $E_i = 73$ meV [48] and thus is not due to the frame overlap problem [52]. Our calculation in Figs. 3(e) and 3(f) cannot explain this scattering around 20 meV. It could be related to magnetic dynamics, since it is clearly observed in the lower $|Q|$ region as with the scattering around (2,2,0) [48]. Figures 3(h)–3(q) illustrate the constant energy cut of the scattering intensity around (2,2,0) and (4,0,0). Figures 3(h)–3(l) are the case of the Mn^{2+} acoustic mode, which is a typical Heisenberg-type spin wave. Since the scattering at 2 meV around the (2,2,0) Γ point [Figs. 3(h)–3(l)] and the scattering at 20 meV around (4,0,0)

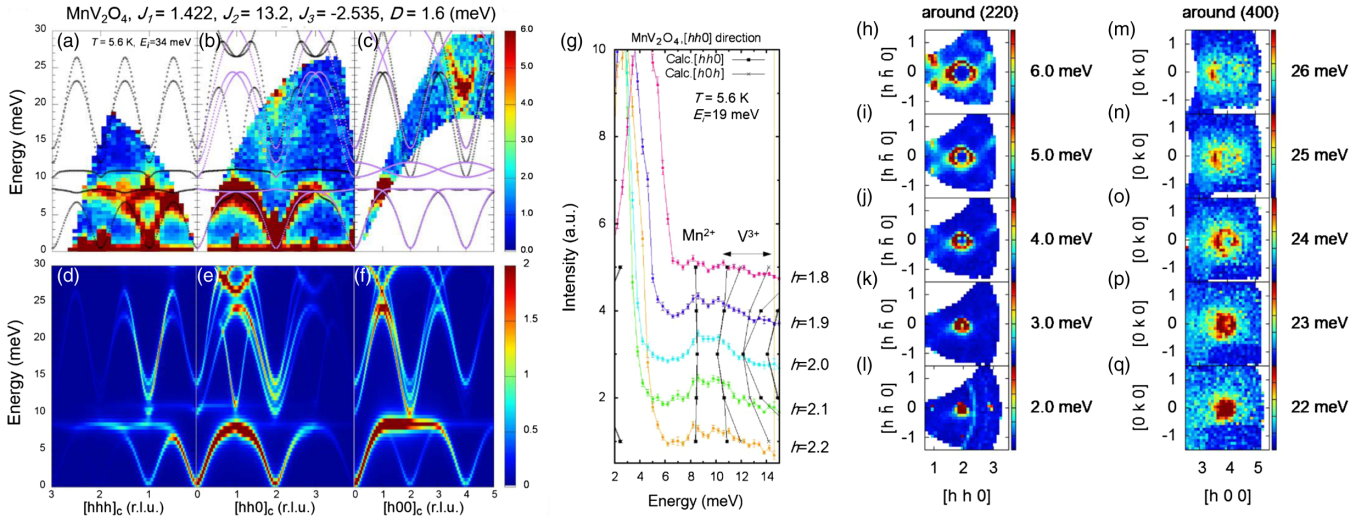

FIG. 3. Experimental inelastic intensity and the corresponding calculated intensity contour along the (a),(d) $[hhh]_c$, (b),(e) $[hh0]_c$, and (c),(f) $[h00]_c$ directions at $T = 5.6$ K. The purple filled and black open circles are the calculated spin wave dispersions along the $[h0h]$ and $[hh0]$ directions in (b) and along the $[00l]$ and $[h00]$ directions in (c), respectively. (g) Plot of inelastic scattering intensity around [220] at $E_i = 19$ meV. The calculated energies of each h value are connected by black lines with a filled circle for the $[hh0]$ modes and with a cross mark for the $[h0h]$ modes. (h)–(k) Inelastic intensity contour in the $[hh0]$-$[h\bar{h}0]$ plane around [220]. The scale is adjusted to that of panels (m)–(q), for comparison. (m)–(q) Inelastic intensity contour in the $[h00]$-$[0k0]$ plane around [400]. These figures were obtained by averaging the data of the $[h00]$-$[0k0]$ and $[h00]$-$[00l]$ planes.

[Figs. 3(m)–3(q)] spread isotropically at higher energy, this 20 meV scattering appears to be a typical spin wave.

The origin of the scattering around 20 meV is discussed below. First, let us consider the excitation at the Γ point. The origin of this scattering has been discussed in several studies on Raman scattering in MnV_2O_4. Miyahara *et al.* observed the peak about 180 cm^{-1} below T_C and interpreted this peak as one-magnon scattering [53] similar to the inelastic scattering observed by Chung *et al.* [26]. Takubo *et al.* observed similar peaks around this energy region below T_C; however, they did not explain the origin of these peaks [54]. Recently, Gleason *et al.* clarified two sharp peaks at 74 cm^{-1} and 84 cm^{-1}, corresponding to one-magnon scattering [30]. The energy width of the 178 cm^{-1} peak, however, was much broader than that of these one-magnon peaks. They argued that the observed broad peak around 20 meV should be ascribed to two-magnon scattering. They also claimed that the anomalous temperature dependence of this two-magnon scattering was due to the spin-lattice coupling [30]. In fact, spin-lattice coupling should be considered for understanding the dynamics in this energy region.

The observed 20 meV scattering, however, is not attributable to two-magnon scattering. The excited energy of two-magnon scattering is generally smaller than the sum of two one-magnon energies, because of its binding energy. In the present case, the sum of two one-magnon energies is at most 20 meV. Thus, the excited energy of the two-magnon scattering is smaller than 20 meV. Generally, two-magnon scattering has no clear dispersion. The propagation of two-magnon scattering corresponds to a higher order term than that of one-magnon scattering in the scattering process. The dispersion of two-magnon scattering is smaller than that of one-magnon scattering. In addition, the neutron scattering intensity of two-magnon scattering is much smaller than the one-magnon scattering intensity, because the total S value is preserved.

We propose that the SOI $\xi\mathbf{l}\cdot\mathbf{s}$ at the V sites affects the energy levels of the magnetic excited state within the first-order perturbation. This effect differs from the anisotropic term D in the Hamiltonian. Using the raising (l^+, s^+), lowering (l^-, s^-), and z-projection (l^z, s^z) operators of orbital $\mathbf{l}$ and spin $\mathbf{s}$ angular momentum, $\xi\mathbf{l}\cdot\mathbf{s}$ can be represented as $\xi\mathbf{l}\cdot\mathbf{s} = (\xi/2)(l^+s^- + l^-s^+) + \xi l^z s^z$. Among the V^{3+} modes (see Fig. 2), V^{3+} mode 6 at ~32 meV with the largest ΔS_z has a larger chance to couple with the orbital excitation through the spin-orbit term. The typical energy scale of the spin-orbit coupling constant ξ in a 3d system is around 10 meV. In mode 6, the maximum length of the spin moment along the z direction S_z at the V sites is about 0.889 [48]; therefore, about 8–9 meV of energy reduction from the calculated energy can be expected. Thus, the discrepancy between the spin wave calculation and the experimental results at the Γ point should be ascribed to the SOI. Interestingly, this spin-orbital correlated excitation might propagate as collective modes [Figs. 4(a), 4(c), and 4(e)]. In the ground state, the projection of the spin moments at the V sites in the z direction is ferromagnetic, as depicted in Figs. 4(c) and 4(d). Let us assume that along the $[\bar{1}01]$ direction [Figs. 4(a) and 4(c)], a neutron flips the $|yz,\uparrow\rangle$ electron at site 1 along the $[\bar{1}01]$ direction to $|yz,\downarrow\rangle$ [Fig. 4(e)]. In this excited state, the SOI $\xi l^z s^z$ would excite the $|yz,\downarrow\rangle$ electron to $|zx,\downarrow\rangle$ as $l^z s^z|yz,\downarrow\rangle = -i|zx,\downarrow\rangle$. This excited state would recover the nonzero orbital angular momentum and gain the energy of the SOI. A spin flip by a neutron can cause an orbital excitation between the $|yz\rangle$ and $|zx\rangle$ orbitals, with the change in spin angular momentum. Furthermore, the $|zx,\downarrow\rangle$ electron at site 1 can be exchanged with the $|zx,\uparrow\rangle$ electron via a direct exchange interaction, leading to the spin-orbital correlated collective mode. Localized orbital excitations could exist in addition to collective spin-orbital excitations. If the $|xy,\uparrow\rangle$ electron at site 1 is flipped to $|xy,\downarrow\rangle$ along the [110] direction [Figs. 4(b) and 4(d)] by a neutron [Fig. 4(f)], the SOI $\xi l^- s^+$ excites the $|xy,\downarrow\rangle$ electron, as $l^- s^+|xy,\downarrow\rangle = |yz,\uparrow\rangle + i|zx,\uparrow\rangle$. The transition to $|yz,\uparrow\rangle$ is forbidden, because $|yz,\uparrow\rangle$ is already occupied. The $|zx,\uparrow\rangle$ electron cannot be transferred to $|yz,\uparrow\rangle$ at site 2, because of the Pauli exclusion rule. This excitation is considered as a localized orbital excitation. Based on the above considerations, we propose that the V^{3+} spin-wave modes would have different energies, taking into account the orbital degree of freedom and SOI. Inelastic polarized neutron scattering and inelastic x-ray scattering

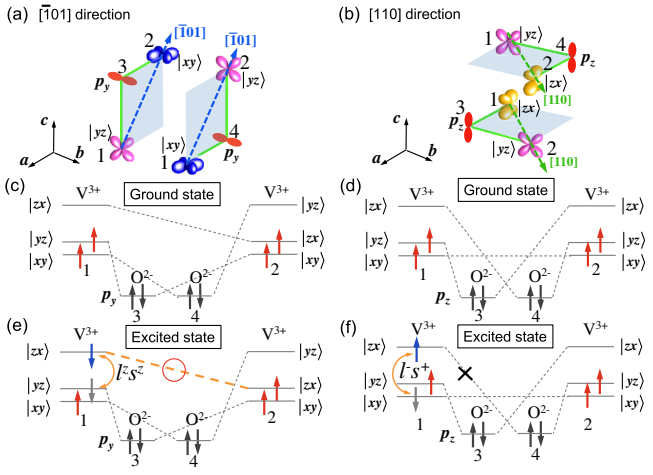

FIG. 4. (a),(b) Schematic figures of superexchange paths via the oxygen $2p$ orbital between neighboring V^{3+} ions for the (a) $[\bar{1}01]_c$ and (b) $[110]_c$ directions. These figures are based on the A-type antiferroic orbital ordering [see also Fig. 1(c)]. The V^{3+} ions are at sites 1 and 2. The surrounding O^{2-} ions are at sites 3 and 4. (c),(d) Electronic structure in the ground state for the (c) $[\bar{1}01]_c$ and (d) $[110]_c$ directions. The spin moments are projected along the z direction. The dotted line indicates the overlapping between orbitals. (e),(f) Excited state along the (e) $[\bar{1}01]_c$ and (f) $[110]_c$ directions.

experiments in a single domain will be required for understanding this spin-wave mode around 20 meV.

In conclusion, the magnetic dynamics in the spinel-type vanadium oxide MnV_2O_4 by INS was investigated. A spin-wave mode was newly observed around 10 meV, which is assigned to V^{3+} spin-wave modes. Using the Heisenberg model with a magnetic anisotropy term, we optimized the values of the magnetic interactions. The scattering around 20 meV cannot be explained with this model, although the calculation can reproduce the lower energy dynamics. We propose that this scattering is due to a V^{3+} spin-wave mode accompanied by orbital excitation. The orbital degree of freedom affects the V^{3+} spin-wave modes.

The neutron experiments were performed at the Materials and Life Science Experimental Facility of the J-PARC under User Programs No. 2012A0058, No. 2013A0141, No. 2014A0113, and No. 2014B0152. This work was supported by JSPS KAKENHI Grant No. JP15K05154. The magnetization measurements were carried out at the Institute for Solid State Physics (ISSP) at the University of Tokyo. We acknowledge T. Masuda, M. Soda, and S. Hayashida for their assistance in taking high-energy Laue photographs at the ISSP. We are grateful to T. Nakajima, N. D. Khanh and Y. Fujima for their helpful comments. K. M. is supported by the Japan Society for the Promotion of Science through the Program for Leading Graduate Schools (MERIT) and a JSPS Research Fellowship for Young Scientists (JSPS KAKENHI Grant No. JP15J08412). The crystal structures were visualized using VESTA3 [55].

*keisuke@cor.k.u-tokyo.ac.jp
†Present address: Max-Planck POSTECH Center for Complex Phase Materials, Pohang University of Science and Technology, Pohang 37673, Republic of Korea.

[1] P. W. Anderson, Science **177**, 393 (1972).
[2] A. Pimenov, A. A. Mukhin, V. Y. Ivanov, V. D. Travkin, A. M. Balbashov, and A. Loidl, Nat. Phys. **2**, 97 (2006).
[3] N. Kida, Y. Takahashi, J. S. Lee, R. Shimano, Y. Yamasaki, Y. Kaneko, S. Miyahara, N. Furukawa, T. Arima, and Y. Tokura, J. Opt. Soc. Am. B **26**, A35 (2009).
[4] Y. Kamihara, T. Watanabe, M. Hirano, and H. Hosono, J. Am. Chem. Soc. **130**, 3296 (2008).
[5] Y. Tokura, Rep. Prog. Phys. **69**, 797 (2006).
[6] N. J. Perks, R. D. Johnson, C. Martin, L. C. Chapon, and P. G. Radaelli, Nat. Commun. **3**, 1277 (2012).
[7] K. Singh, C. Simon, E. Cannuccia, M.-B. Lepetit, B. Corraze, E. Janod, and L. Cario, Phys. Rev. Lett. **113**, 137602 (2014).
[8] Y. Tokura and N. Nagaosa, Science **288**, 462 (2000).
[9] E. Saitoh, S. Okamoto, K. T. Takahashi, K. Tobe, K. Yamamoto, T. Kimura, S. Ishihara, S. Maekawa, and Y. Tokura, Nature (London) **410**, 180 (2001).
[10] J. van den Brink, Phys. Rev. Lett. **87**, 217202 (2001).
[11] K. Ishii, S. Ishihara, Y. Murakami, K. Ikeuchi, K. Kuzushita, T. Inami, K. Ohwada, M. Yoshida, I. Jarrige, N. Tatami, S. Niioka, D. Bizen, Y. Ando, J. Mizuki, S. Maekawa, and Y. Endoh, Phys. Rev. B **83**, 241101 (2011).
[12] C. Ulrich, A. Gössling, M. Grüninger, M. Guennou, H. Roth, M. Cwik, T. Lorenz, G. Khaliullin, and B. Keimer, Phys. Rev. Lett. **97**, 157401 (2006).
[13] C. Ulrich, G. Ghiringhelli, A. Piazzalunga, L. Braicovich, N. B. Brookes, H. Roth, T. Lorenz, and B. Keimer, Phys. Rev. B **77**, 113102 (2008).
[14] S. Miyasaka, S. Onoda, Y. Okimoto, J. Fujioka, M. Iwama, N. Nagaosa, and Y. Tokura, Phys. Rev. Lett. **94**, 076405 (2005).
[15] S. Miyasaka, J. Fujioka, M. Iwama, Y. Okimoto, and Y. Tokura, Phys. Rev. B **73**, 224436 (2006).
[16] J. Schlappa, K. Wohlfeld, K. J. Zhou, M. Mourigal, M. W. Haverkort, V. N. Strocov, L. Hozoi, C. Monney, S. Nishimoto, S. Singh, A. Revcolevschi, J.-S. Caux, L. Patthey, H. M. Ronnow, J. van den Brink, and T. Schmitt, Nature (London) **485**, 82 (2012).
[17] L. Mittelstädt, M. Schmidt, Z. Wang, F. Mayr, V. Tsurkan, P. Lunkenheimer, D. Ish, L. Balents, J. Deisenhofer, and A. Loidl, Phys. Rev. B **91**, 125112 (2015).
[18] K. Matsuno, T. Katsufuji, S. Mori, Y. Moritomo, A. Machida, E. Nishibori, M. Takata, M. Sakata, N. Yamamoto, and H. Takagi, J. Phys. Soc. Jpn. **70**, 1456 (2001).
[19] S.-H. Lee, D. Louca, H. Ueda, S. Park, T. J. Sato, M. Isobe, Y. Ueda, S. Rosenkranz, P. Zschack, J. Íñiguez, Y. Qiu, and R. Osborn, Phys. Rev. Lett. **93**, 156407 (2004).
[20] H. Mamiya, M. Onoda, T. Furubayashi, J. Tang, and I. Nakatani, J. Appl. Phys. **81**, 5289 (1997).
[21] S. Niitaka, H. Ohsumi, K. Sugimoto, S. Lee, Y. Oshima, K. Kato, D. Hashizume, T. Arima, M. Takata, and H. Takagi, Phys. Rev. Lett. **111**, 267201 (2013).
[22] G. Giovannetti, A. Stroppa, S. Picozzi, D. Baldomir, V. Pardo, S. Blanco-Canosa, F. Rivadulla, S. Jodlauk, D. Niermann, J. Rohrkamp, T. Lorenz, S. Streltsov, D. I. Khomskii, and J. Hemberger, Phys. Rev. B **83**, 060402 (2011).
[23] K. Adachi, T. Suzuki, K. Kato, K. Osaka, M. Takata, and T. Katsufuji, Phys. Rev. Lett. **95**, 197202 (2005).
[24] T. Suzuki, M. Katsumura, K. Taniguchi, T. Arima, and T. Katsufuji, Phys. Rev. Lett. **98**, 127203 (2007).
[25] V. O. Garlea, R. Jin, D. Mandrus, B. Roessli, Q. Huang, M. Miller, A. J. Schultz, and S. E. Nagler, Phys. Rev. Lett. **100**, 066404 (2008).
[26] J.-H. Chung, J.-H. Kim, S.-H. Lee, T. J. Sato, T. Suzuki, M. Katsumura, and T. Katsufuji, Phys. Rev. B **77**, 054412 (2008).
[27] J.-H. Chung, J.-H. Kim, S.-H. Lee, T. J. Sato, T. Suzuki, M. Katsumura, and T. Katsufuji, Phys. Rev. B **87**, 139907(E) (2013).
[28] Y. Nii, H. Sagayama, T. Arima, S. Aoyagi, R. Sakai, S. Maki, E. Nishibori, H. Sawa, K. Sugimoto, H. Ohsumi, and M. Takata, Phys. Rev. B **86**, 125142 (2012).
[29] Y. Nii, N. Abe, and T.-h. Arima, Phys. Rev. B **87**, 085111 (2013).
[30] S. L. Gleason, T. Byrum, Y. Gim, A. Thaler, P. Abbamonte, G. J. MacDougall, L. W. Martin, H. D. Zhou, and S. L. Cooper, Phys. Rev. B **89**, 134402 (2014).

[31] K. Matsuura, H. Sagayama, Y. Nii, N. D. Khanh, N. Abe, and T. Arima, Phys. Rev. B **92**, 035133 (2015).
[32] T. Katsufuji, T. Suzuki, H. Takei, M. Shingu, K. Kato, K. Osaka, M. Takata, H. Sagayama, and T. hisa Arima, J. Phys. Soc. Jpn. **77**, 053708 (2008).
[33] G. J. MacDougall, V. O. Garlea, A. A. Aczel, H. D. Zhou, and S. E. Nagler, Phys. Rev. B **86**, 060414 (2012).
[34] G. J. MacDougall, I. Brodsky, A. A. Aczel, V. O. Garlea, G. E. Granroth, A. D. Christianson, T. Hong, H. D. Zhou, and S. E. Nagler, Phys. Rev. B **89**, 224404 (2014).
[35] Q. Zhang, M. Ramazanoglu, S. Chi, Y. Liu, T. A. Lograsso, and D. Vaknin, Phys. Rev. B **89**, 224416 (2014).
[36] Y. Huang, Z. Yang, and Y. Zhang, J. Phys. Condens. Matter **24**, 056003 (2012).
[37] R. Koborinai, S. E. Dissanayake, M. Reehuis, M. Matsuda, T. Kajita, H. Kuwahara, S.-H. Lee, and T. Katsufuji, Phys. Rev. Lett. **116**, 037201 (2016).
[38] D. Reig-i-Plessis, D. Casavant,V. O. Garlea,A. A. Aczel, M. Feygenson, J. Neuefeind, H. D. Zhou, S. E. Nagler, and G. J. MacDougall, Phys. Rev. B **93**, 014437 (2016).
[39] K. I. Kugel and D. I. Khomski, Sov. Phys. Usp. **25**, 231 (1982).
[40] Y. Motome and H. Tsunetsugu, Prog. Theor. Phys. Suppl. **160**, 203 (2005).
[41] S. Ishihara, Phys. Rev. B **69**, 075118 (2004).
[42] Y. Nii, N. Abe, K. Taniguchi, and T. Arima, Appl. Phys. Lett. **100**, 051905 (2012).
[43] H. Tsunetsugu and Y. Motome, Phys. Rev. B **68**, 060405 (2003).
[44] R. Kajimoto *et al.*, J. Phys. Soc. Jpn. **80**, SB025 (2011).
[45] M. Russina and F. Mezei, Nucl. Instrum. Methods Phys. Res., Sect. A **604**, 624 (2009).
[46] M. Nakamura, R. Kajimoto, Y. Inamura, F. Mizuno, M. Fujita, T. Yokoo, and M. Arai, J. Phys. Soc. Jpn. **78**, 093002 (2009).
[47] Y. Inamura, T. Nakatani, J. Suzuki, and T. Otomo, J. Phys. Soc. Jpn. **82**, SA031 (2013).
[48] See Supplemental Material at http://link.aps.org/supplemental/10.1103/PhysRevLett.119.017201 for the details of experiment and calculation, which includes Refs. [25–28,31,49–51].
[49] J. Okabayashi *et al.* reported $\langle L_z \rangle \sim 0.15$ in a 5 T magnetic field. [J. Okabayashi, S. Miyasaka, K. Hemmi, K. Tanaka, S. Tajima, H. Wadati, A. Tanaka, Y. Takagi, and T. Yokoyama, J. Phys. Soc. Jpn. **84**, 104703 (2015)].
[50] N. B. Perkins and O. Sikora, Phys. Rev. B **76**, 214434 (2007).
[51] Y. Yafet and C. Kittel, Phys. Rev. **87**, 290 (1952).
[52] G. E. Granroth, J. Phys. Soc. Jpn. **80**, SB016 (2011).
[53] S. Miyahara, K. Takubo, T. Suzuki, T. Katsufuji, and N. Furukawa, arXiv:1012.4073.
[54] K. Takubo, R. Kubota, T. Suzuki, T. Kanzaki, S. Miyahara, N. Furukawa, and T. Katsufuji, Phys. Rev. B **84**, 094406 (2011).
[55] K. Momma and F. Izumi, J. Appl. Crystallogr. **44**, 1272 (2011).